AGU PUBLICATIONS

Geophysical Research Letters

RESEARCH LETTER
10.1002/2015GL066082

Key Points:
- Development of new model which reproduces spatial dependence of aftershocks
- Aftershocks show reduced stress drops explaining puzzling GMPE observations
- Lower stress drops arise from rerupturing incompletely healed fault

Supporting Information:
- Text S1, Table S1, and Figures S1–S6

Correspondence to:
B. E. Shaw,
shaw@ldeo.columbia.edu

Citation:
Shaw, B. E., K. Richards-Dinger, and J. H. Dieterich (2015), Deterministic model of earthquake clustering shows reduced stress drops for nearby aftershocks, *Geophys. Res. Lett.*, *42*, 9231–9238, doi:10.1002/2015GL066082.

Received 8 SEP 2015
Accepted 5 OCT 2015
Accepted article online 22 OCT 2015
Published online 6 NOV 2015

Deterministic model of earthquake clustering shows reduced stress drops for nearby aftershocks

Bruce E. Shaw[1], Keith Richards-Dinger[2], and James H. Dieterich[2]

[1]Lamont Doherty Earth Observatory, Columbia University, Palisades, New York, USA, [2]Department of Earth Sciences, University of California, Riverside, California, USA

Abstract While a number of viable physical mechanisms have been offered to explain the temporal clustering of aftershocks, the spatial clustering of aftershocks, in particular the concentrated productivity of aftershocks very near the mainshock rupture area, has been difficult to reproduce with physical models. Here we present a new deterministic physical model capable of reproducing both the spatial and temporal clustering. We apply this new model to a longstanding puzzling question raised by ground motion observations, which suggest that nearby aftershocks show reduced ground motions relative to similar magnitude mainshocks. In the model, the physical basis for these observations is reduced stress drops for nearby aftershocks compared to similar magnitude mainshocks. These reduced stress drops are due to nearby aftershocks rerupturing incompletely healed parts of the fault which ruptured in the mainshock.

1. Introduction

Earthquakes cluster intensely in time and space. While many aspects of earthquake aftershocks have been well characterized, some fundamental features remain poorly understood. Statistical models have reproduced many of the temporal and spatial clustering features of aftershocks and foreshocks [*Ogata*, 1988; *Helmstetter and Sornette*, 2002; *Felzer et al.*, 2004; *Helmstetter et al.*, 2005; *Sornette and Werner*, 2005; *Marsan and Lengline*, 2008; *Powers and Jordan*, 2010] and enabled useful associated statistical predictions [*Kagan and Knopoff*, 1981; *Ogata*, 1988; *Reasenberg and Jones*, 1989; *Gerstenberger et al.*, 2005]. A number of candidate physical processes of their origin have been proposed [*Dieterich*, 1994; *Huc and Main*, 2003; *Perfettini and Avouac*, 2007; *Helmstetter and Shaw*, 2009], so there is a good basis for exploring how their phenomenology fits with our understandings. While many of the proposed physical processes give consistent temporal behavior reproducing the central basic Omori law ($1/t$) time dependence in the rate of events [*Das and Scholz*, 1981; *Dieterich*, 1994; *Shaw*, 1993], reproducing the spatial distribution of aftershocks has turned out to be a much more difficult challenge for physical models. In particular, the observation that aftershocks occur not only in the regions outside the rupture area but prolifically nearby inside the rupture area as well has been a great challenge to reproduce in physical models (though statistical models put this in by hand).

A further challenge in trying to understand aftershocks physically is that some observations suggest that ground motions of aftershocks are reduced, statistically, relative to similar sized mainshocks [*Boore and Atkinson*, 1989]. More recent compilations based on broader data sets have led groups to differing conclusions, with some groups finding reduced ground motions for nearby aftershocks [*Abrahamson and Silva*, 2008; *Abrahamson et al.*, 2014; *Chiou and Youngs*, 2008] and other groups not [*Boore et al.*, 2014]. Are nearby aftershocks then somehow different from mainshocks? Given the lack of consensus on these ground motion results [*Abrahamson et al.*, 2008; *Gregor et al.*, 2014], the use of these regressions in building codes, and the challenges to our understanding of aftershock phenomena, a better physical understanding of these events would be very welcome.

In this paper we present a new model which deterministically reproduces a variety of observed statistical properties of aftershocks, including in particular the nearby spatial population of aftershocks. These nearby aftershocks in the model have, on average, reduced stress drops relative to mainshocks of similar magnitude. Reduced stress drops for these aftershocks was discussed as an origin for the reduced ground motions observations in the original observations [*Boore and Atkinson*, 1989] and has been shown to be consistent with other features of the ground motions in recent work [*Baltay et al.*, 2013]. With our new model, we find a

physical source and explanation for this puzzling phenomena, giving a new tool to explore aftershock behavior, and a basis for understanding how to better estimate societally important ground motions.

2. Model

A number of statistical and physical models have been developed to reproduce observed statistical clustering regularities. The statistical models have found many uses but also have limitations. Leading models such as ETAS (Epidemic Type Aftershock Sequence) have run into difficulties when attempts have been made to integrate with longer term models due to difficulties with elastic rebound effects [*Field et al.*, 2014]. Recent work by *Shearer* [2012a, 2012b] has pointed to the difficulty commonly used statistical models have trying to match productivity and spatial and temporal distributions of observed seismicity. Other recent work has called into question a typically used simplification in the statistical models that the spatial and magnitude distributions are separable; instead, larger aftershocks were found to occur almost exclusively outside the mainshock rupture area, breaking separability and suggesting the presence of elastic rebound effects [*van der Elst and Shaw*, 2015]. Statistical models also do not provide any guidance regarding the questions raised by the different ground motion models on whether or not nearby aftershocks differ from mainshocks. They can of course build in such an effect—or not—but do not answer the question of whether such an effect exists. Aiming for a physical explanation of the production of aftershocks near the mainshock surface which has slipped, Dieterich, along with coworkers [*Dieterich*, 2007; *Dieterich and Smith*, 2009; *Smith and Dieterich*, 2010], has suggested that fault roughness [*Power et al.*, 1988] may play a fundamental role in producing highly heterogeneous stresses adjacent to the fault rupture surface, which can drive aftershocks in the interior region of the mainshock rupture. While several statistical implications of these ideas have been explored, those models fail to produce aftershocks that rerupture the mainshock rupture surface, a feature we will see in this work is a significant limitation. Additionally, implementing these ideas in numerical simulations of the full earthquake cycle in a way which could reproduce the spatial features has remained an unachieved goal.

Our new physical model is based on a generalization of an extremely efficient quasi-static boundary element model developed by *Dieterich and Richards-Dinger* [2010]. Some details of the model and its approximations are presented in the supporting information; a key aspect is that it preserves the fundamental features of the rate and state friction equations, which lead to delayed time-to-failure nucleation effects and temporal clustering [*Dieterich*, 1994]. The model makes three key assumptions. First, elements interact with quasi-static elastic interactions, so dynamic stresses are neglected. Second, rate-and-state frictional behavior is simplified into a three regime system where elements are either stuck, nucleating, or sliding dynamically. Third, during dynamic sliding slip rate is fixed at a constant sliding rate. These approximations allow for analytic treatments of rate and state behaviors in different sliding regimes and a tremendous speed-up computationally. *Richards-Dinger and Dieterich* [2012] have presented a number of favorable comparisons of this model with fully dynamic simulations and observations, though they are, of course, not equivalent. Our current model extends this model in two crucial ways. First, we have generalized the model to allow for remote loading, rather than the more traditional methods using backslip loading. This new loading allows the model to self-organize slip onto structures, rather than reproducing a specified rate of slip. A second feature of our generalization is the introduction of multistranded faults, taking a fault to be not a single surface but a braided anastomosing system of surfaces. The multistranded aspect of faults is often noted in observations [*Schaff et al.*, 2002; *Shearer*, 2002; *Hickman et al.*, 2005; *Bryant*, 2005; *Lin et al.*, 2007; *Madden and Pollard*, 2012] but has generally not been included in modeling efforts [*Ely et al.*, 2009; *Dunham et al.*, 2011]. One reason for this may be that it presents substantial difficulties for many numerical methods, such as finite elements and finite differences, since it requires the ability to simulate closely spaced low angled surfaces. It is a significant virtue of our methodology that it can handle these situations. Multiple strands are important for a number of reasons. First, it substantially reduces the tendency of rough faults to lock up [*Dieterich and Smith*, 2009], providing complementary extensional and compressional bends on neighboring strands to accommodate shear motion. Figure 1 illustrates this effect, comparing the slip rate the system chooses under the same constant stress rate remote loading conditions, in one case for single-strand geometry, and in the other case for multiple strands. Note the more crack-like (planar fault-like) slip occurring across the multistranded system in Figure 1b.

Two features of the computational framework extend what is already a very exciting deformational capability to a whole new set of possibilities. First, the deformation occurs in individual stick slip events, showing a wide ranging complexity with many earthquake-like features [*Richards-Dinger and Dieterich*, 2012]. Second, the approximations of the rate state equations preserve the temporal clustering features arising from the

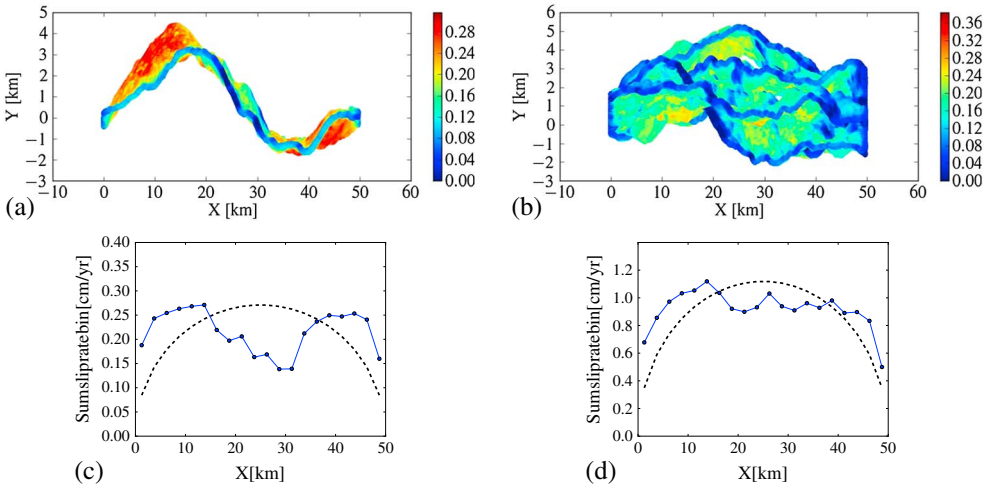

Figure 1. Single-strand versus multistrand fault system geometry. Fault geometry is shown in Figures 1a and 1b. Slip rate summed across fault system width is shown in Figures 1c and 1d. (a) Single-strand fault geometry. Color scale shows slip rate in cm/yr. View is looking up from the bottom of the faults; there is more slip at the top free surface. The fault-perpendicular *Y* axis is magnified relative to the fault-parallel *X* axis to illuminate roughness features. (b) Multiple strands. (c) Single strand, slip rate summed across directions *Y* and vertical *Z*. Dashed line shows crack solution set to maximum slip amplitude. (d) Multiple strands, slip rate summed across directions *Y* and vertical *Z*. Note in the slip rates on the bottom how the multistrand (Figure 1d) is more crack-like in its summed slip across the fault zone, while the single strand (Figure 1c) is tending to slip less and lock up.

nucleation process [*Dieterich*, 1994]. Thus, out of this interesting deformation environment arises a complex space-time catalog of events, a rich seismicity with interesting behaviors across multiple space and time scales.

3. Aftershocks

Computing earthquake behavior on a range of timescales in a self-consistent way allows us to analyze how the statistical properties of aftershock sequences emerge from the fundamental physical properties of the model. We are able to simulate long sequences of clustered events over a whole range of time and space scales, as Figure 2 illustrates. Note the crucial feature, illustrated in Figure 2b, that there are substantial numbers of aftershocks happening within the area which ruptured during the mainshock, something missing in simpler single fault surface models.

To be more quantitative, we stack sequences of moderate magnitude events, which can then be compared with observations. For simplicity, we use restrictive criteria for selecting mainshocks and aftershocks, discarding events with more ambiguity, since completeness in identification is not needed for our purposes. To identify a subset of events as mainshocks, we fix a time window before and after an event and require that no event larger than the mainshock have occurred in the preceding time window over a specified large length scale. We set these selection criteria conservatively, so that we are discarding many potential mainshocks but retaining a clear unambiguous set of mainshocks (see supporting information for details). The model aftershocks show a number of features which are quite consistent with observed earthquake aftershock behavior. The decay of the rate of aftershocks following the stacked mainshocks in the model (Figure 3a) follows a power law with an exponent slightly less than unity, consistent with Omori's law for observed aftershock sequences [*Dieterich*, 1994; *Shaw*, 1993]. There is also good quantitative agreement between the observations (Figure 3b) [*Shaw*, 1993; *Shearer*, 2012a] and the model (Figure 3c) in the magnitude-dependent productivity of aftershocks and the contrast with the preceding foreshocks. Other features of the modeled aftershocks also compare well with observations, including Bath's law relating the largest magnitude aftershock relative to the mainshock, and the distribution of sizes of events, which is a Gutenberg-Richter power law behavior in moment for the small events, along with a characteristic peak of large events above the extrapolated small events rate (see supporting information).

The magnitude-dependent productivities for the foreshocks and aftershocks do have some sensitivities to a few model parameters. Parameters in the model include rupture parameters and fault geometry parameters. Stress drops are set by the rate-and-state friction parameters and an overall normal stress. The most

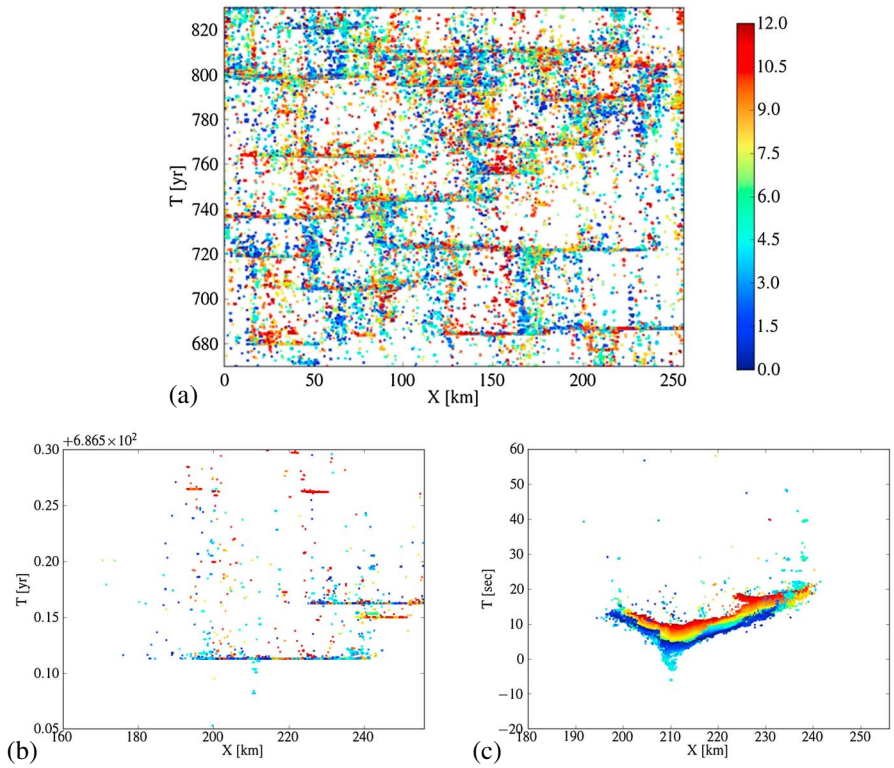

Figure 2. Seismicity in a multistranded model on wide range of timescales. Horizontal axis is distance along faults in kilometers. Vertical axis is time, with successive subfigures showing zooms into shorter time scales. Color denotes depth of rupture on an element, in units of kilometers, with red deep and blue shallow. (a) Century timescale. (b) Years, showing aftershocks happening along rupture area. (c) Seconds, showing dynamic rupture and initial early aftershocks. Same event as lower large event in Figure 2b. Note spatial temporal clustering of events. Note also aftershocks happening after large events along the rupture area.

important parameter affecting the relative aftershock productivity is *a*, the coefficient of the logarithmic rate term in the rate-and-state friction constitutive law [*Dieterich*, 1994]. Increasing *a* increases the rate of aftershocks. This occurs because many aftershocks happen when parts of faults which might have been recruited to fail coseismically are delayed in their time to failure with larger *a* and instead fail postseismically

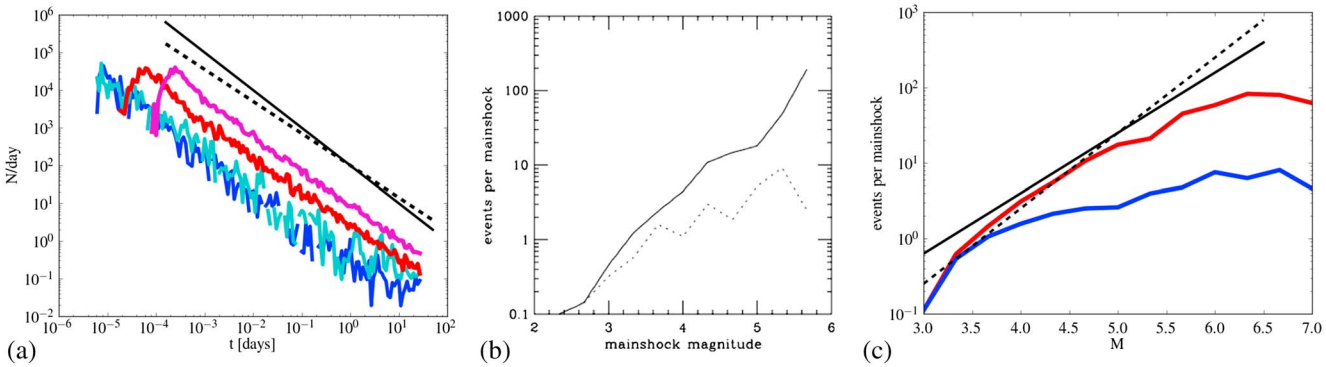

Figure 3. Productivity measures of aftershocks. (a) Omori law time dependence in the model. Number of events as a function of time following mainshock initiation time. Aftershocks of *M*5 and *M*6 mainshocks are red and magenta curves, respectively. Foreshocks of *M*5 and *M*6 mainshocks are blue and cyan curves, respectively. The finite duration of the mainshocks is reflected in the time of earliest onset of the aftershocks. Black solid line shows $p = 1$ slope Omori law. Black dashed line shows $p = 0.85$ slope for reference. Note that decay has $p < 1$, in agreement with observations [*Dieterich*, 1994]. Note also magnitude dependence of aftershock productivity and larger difference between number of foreshocks and aftershocks for larger magnitude mainshocks. (b) Number of foreshocks and aftershock events above a cut-off magnitude in a fixed space-time window as a function of mainshock magnitude for earthquake data from Northern California from *Shaw* [1993]. (c) Number of foreshocks and aftershocks as a function of mainshock magnitude in the model. Blue line shows foreshocks, and red line shows aftershocks. Dashed black line shows slope 1, and solid black line shows slope 0.8.

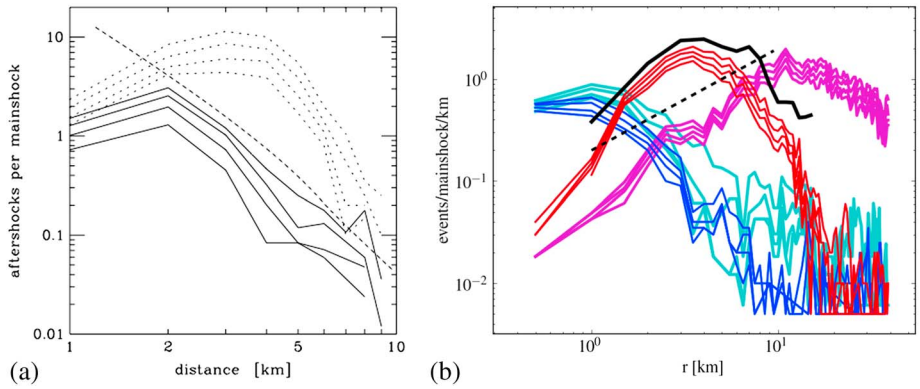

Figure 4. Aftershock spatial distribution. Linear density of aftershocks as a function of distance from the mainshock hypocenter. (a) Earthquake data from Northern California from *Shaw* [1993]. Solid lines are for magnitude 4 mainshocks, with different curves being cumulative events at increasing time intervals, and thin dashed lines are for magnitude 5 mainshocks. Thicker dashed line is a theoretical curve combining finite seismogenic thickness with a $1/r^3$ static stress kernel [*Shaw*, 1993]. (b) Model data. Here foreshocks and aftershocks of magnitudes 5 and 6 mainshocks are shown. Blue lines are foreshocks of *M*5 mainshocks. Cyan lines are foreshocks of *M*6 mainshocks. Interestingly, there are slightly more foreshocks in the extended area of the future *M*6 mainshocks relative to the *M*5 mainshocks. The main focus is, however, the aftershocks. Red lines are aftershocks of *M*5 mainshocks; magenta lines are aftershocks of *M*6 mainshocks. Again, different curves are cumulative events at increasing time intervals. Dashed black line shows constant surface density, a linear increase in linear density. Thick black line shows, for comparison, spatial distribution of aftershocks from observed *M*5 mainshocks; note how red model *M*5 mainshock lines compare favorably with thick black earthquake data line for the spatial dependence.

as aftershocks. The best comparisons with observations occurred for quite small a values, $a = 0.00025$ or $a\sigma = 0.025$ MPa with a normal stress of $\sigma = 100$ MPa. These a values are much smaller than typical lab values [*Dieterich*, 1994] but consistent with other low values of $a\sigma$ inferred from aftershock observations [e.g., *Toda et al.*, 2005]. Other rupture parameters appear much less important; a full discussion of parameters and their sensitivities is presented in the supporting information. For fault geometry parameters, some degree of roughness is important, but the dependence on roughness is quite weak. Multistrands are important for getting the productivity right, especially at larger magnitudes. Aftershocks do occur on single strands, but the rates of aftershocks on the interior areas of moderate and larger sized mainshocks are very low for single-stranded faults. Again, a fuller discussion of parameters is presented in the supporting information, but the key qualitative results we present in this paper hold generically. While the productivity does have some parameter sensitivity, we can find sets of model parameters which appear to do a good job matching the observations, and this is, as far as we are aware, a new achievement for deterministic models.

4. Spatial Distribution of Aftershocks

Stacking the aftershocks of similar sized mainshocks, we can examine the spatial distribution of aftershocks for both actual California data (Figure 4a) and the model data (Figure 4b). For the range of mainshock magnitudes where we have the capability to best make comparisons (small enough to have many events and thus good observational statistics and large enough to have enough spatial resolution in the model to have a broad population of smaller aftershocks), we see very promising results, as the consistency of the solid black data line and the thick red model line for magnitude 5 mainshocks show in Figure 4b. Higher grid resolution gives more aftershocks, since the minimum magnitude decreases as the grid becomes more resolved, so it is the shape of the curves which are the important comparison here.

5. Nearby Aftershocks

Ground motion prediction equations (GMPEs) are empirically based equations giving parameterized expected levels of shaking as a function of magnitude, distance, and source mechanism for earthquakes. They play a central role in engineering applications for estimating expected shaking and design criteria. Based on regressions of recorded seismic records of past earthquakes, they provide a benchmark description of median ground motions and variability about the median. In recent community efforts at updating these relations, a number of prominent groups have found reduced ground motions for nearby aftershocks

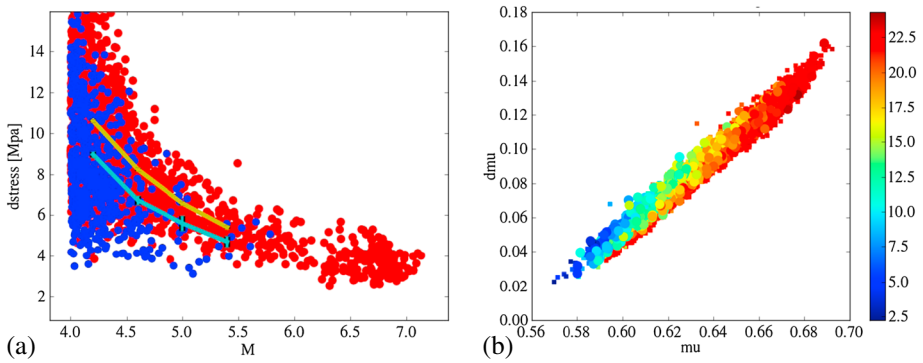

Figure 5. Lower median stress drops for nearby aftershocks relative to mainshocks in model. (a) Mean stress drops averaged over rupture area as a function of magnitude. Red circles are averages for individual mainshocks, and blue circles are averages for individual nearby aftershocks. The blue circles tending to lie below the red circles at a given magnitude illustrate the differences in the statistics of the populations. Solid lines show averages for a given magnitude of the two populations, with yellow showing mainshocks and cyan showing nearby aftershocks. Systematic lowering is shown by cyan curve lying below yellow curve. Error bars on curves show one standard error uncertainty in mean. (b) Physical origin for the lower mean stress drops of nearby aftershocks. The effect comes from nearby aftershocks rerupturing portions of recent mainshock areas which are early in their rehealing process and thus have lower dynamic strength drops. Plot shows friction drop versus initial friction value, averaged over source area for individual events. Colors show average of the natural log of state variable in seconds (the state variable heals linearly with time when stuck in the rate-and-state equations used here). The blue points in the bottom left show events which have been stuck for a shorter time and thus tend to have a lower strength drop when they rerupture relative to the parts of the fault which have been stuck a long time, shown in red points.

[*Abrahamson and Silva*, 2008; *Abrahamson et al.*, 2014; *Chiou and Youngs*, 2008]. To give a sense of the scale of the effect, in the *Abrahamson et al.* [2014] relation this effect is a reduction of 0.3 in the natural logarithm of the high-frequency ground motion. This is a substantial enough effect, in terms of implied signal, and engineering implications, that an explanation for why it is appearing in the regressions is important to understand. It is also a very puzzling effect. Are aftershocks fundamentally different physically? Are there biases in the data sets? Are such corrections sufficiently solidly based as to make design decisions on? Why are some groups seeing an effect [*Abrahamson and Silva*, 2008; *Abrahamson et al.*, 2014; *Chiou and Youngs*, 2008] and others not [*Boore et al.*, 2014]? Statistical seismicity models have thus far not incorporated such effects into synthetic catalogs. They could, or not, but again, they contain what is put into them, not tell us what the ingredients ought to be. Physical models, on the other hand, do have the potential to address such questions. An absence of such an effect would not rule it out, as many potential physical effects are missing in such models. But its presence, on the other hand, would be a different matter. Then, its origin would be important to understand.

Motivated by this important question, we have explored this issue in the model, comparing nearby aftershocks with mainshocks of similar magnitude. We give full details of the mainshock and nearby aftershock selection criteria in the supporting information and here only note that we consider aftershocks to be nearby if their hypocenters occur within a distance of the mainshock hypocenter which scales as the mainshock magnitude, with the distance chosen to be around a diameter typical of the mainshock magnitude. This nearby distance as a function of mainshock magnitude M is taken to be: $R_{\text{nearby}} = 1.1 \times 10^{(M-4)/2}$ km. Though this is not the same criteria as used in the NGA measures of Class II events (nearby aftershocks) [*Gregor et al.*, 2014] it is easy to implement and captures a similar idea of looking at spatially and temporally nearby events.

Figure 5 illustrates our new findings that indeed, the population of nearby aftershocks shows lower stress drops than that of comparable magnitude mainshocks. Figure 5a plots the stress drops for individual events averaged over their rupture areas plotted against their magnitudes, with mainshocks in red and nearby aftershocks in blue. There is a systematic shift between the population of stress drops, with the nearby aftershocks lying on average below the mainshocks. While the differences are only a fraction of the means, they are important physically and practically and are statistically significant, with the uncertainties in the mean (shown by error bars in the plot) being less than the separation of the means. This supports an early idea based on limited observational data that stress drops for aftershocks might be lower [*Boore and Atkinson*, 1989]; the reason for this effect, however, as Figure 5b shows, differs from that early speculation, which they attributed to areas of reduced stress. It also is consistent with more recent examinations of this question which have also found

lower stress drops for aftershocks [*Baltay et al.*, 2011, 2013]. In addition to reproducing these observations, what is especially interesting about our model is that we have found a physical basis for this effect. Figure 5b gives an explanation for why the nearby aftershocks are exhibiting reduced stress drops in the model. It is essentially coming from the fact that nearby aftershocks are frequently rerupturing parts of the fault which have recently ruptured, and those parts have lower strength drops due to the slow rehealing of faults, a feature present in the laboratory-based rate-and-state friction used in the model which heals logarithmically in time. Figure 5b plots for individual events an average over the rupture area of the drop in friction coefficient against the initial friction coefficient at the start of the event. Due to the rate-and-state friction used in the model, during a dynamic event the friction drops to an approximately constant dynamic value (with a slight dynamic overshoot), so unsurprisingly there is a linear trend of friction drop with initial friction. The points are color coded by the log of the state variable averaged over the rupture area. The color coding makes evident the effect: cold blue colors, indicating low state variable and short healing times, have smaller initial strengths relative to the dynamic strength and thus lower strength drops. The blue points are concentrated in the lower left corner. These are the low strength drop, low stress drop events. A clear physical mechanism underlies this important low stress drop nearby aftershock effect. These results in Figure 5 of lowered friction drops of nearby aftershocks, and its basis in the rerupturing of mainshock rupture area holds generically in the model. This is, to our knowledge, the first theoretical indication of replication of the theoretically surprising empirical observations of reduced shaking of nearby aftershocks.

A further examination of the state variables where events initiate adds some additional insight into the spatial relationships of the low stress drop aftershocks to the mainshocks. Figure 5b shows that there is a strong association between low friction drop events with low average state variable due to having recently ruptured and incomplete healing. Looking at the hypocenters where these events initiate, however, we find that for low mean state variable events (those with average $\overline{\ln \theta} < \ln T_c$ with $T_c = e^{13}$ s ≈ 30 days) the fraction of hypocenters also having low state variable values is very small, 0.15 for the catalog in Figure 5. That is, the vast majority of the events which do rerupture recently ruptured areas start from an area which did not rupture recently. Thus, these nearby low stress drop aftershocks are typically initiating at recently unruptured sites and then propagating onto recently ruptured areas. Further details of the spatial distribution of initiation points are given in the supporting information, but the main message is that aftershocks mainly initiate at points which did not rupture in the mainshock, be they on the main rupture strand or on adjacent strands, but then lower average stress drops occur if the expanding aftershock reruptures parts of the mainshock rupture area.

Finally, some physical consistency of this explanation of low ground motions based on rebreaking incompletely healed faults can also be examined. The rehealing of faults based on rate-and-state friction occurs logarithmically in time. For logarithmic healing, the healing which takes place between 1 s and 2 days is comparable to the healing which takes place between 2 days and a thousand years. Thus, after 2 days, we are roughly halfway healed in the earthquake cycle. Thus, this effect could explain of order a factor of 2 difference in stress drops of aftershocks relative to mainshocks, but certainly not a factor of 10 or more. As noted earlier, however, while the details of the nearby aftershock effect in the GMPE regressions is not simple, the *Abrahamson et al.* [2014] relation shows around a 25% reduction for the class II event (nearby aftershock) high-frequency shaking, a value which as an average includes events showing this effect and not. Thus, the size of the observed effect is well within the expected scale range of a logarithmic healing explanation and is comparable to the difference in median stress drops seen in the model data. This first initial application of our newly introduced model which deterministically produces complex aftershock sequences illustrates its great potential as a tool in studying earthquake clustering phenomena beyond assumed statistical properties.

Acknowledgments

We thank Gail Atkinson and an anonymous reviewer for helpful comments which improved the manuscript. This work was supported by NSF grants EAR-0943939, EAR-1135455, EAR-1447094, and TG-EAR130035 and by the Southern California Earthquake Center (SCEC). Heming Xu provided assistance in running early versions of the model. New model data and older earthquake catalog data available from corresponding author upon request.

References

Abrahamson, N., and W. Silva (2008), Summary of the Abrahamson & Silva NGA ground-motion relations, *Earthquake Spectra*, *24*, 67–97.

Abrahamson, N., G. Atkinson, D. Boore, Y. Bozorgnia, K. Campbell, B. Chiou, I. M. Idriss, W. Silva, and R. Youngs (2008), Comparisons of the NGA ground-motion relations, *Earthquake Spectra*, *24*, 45–66.

Abrahamson, N. A., W. J. Silva, and R. Kamai (2014), Summary of the ASK14 ground-motion relation for active crustal regions, *Earthquake Spectra*, *30*, 1025–1055.

Baltay, A. S., S. Ide, G. Prieto, and G. Beroza (2011), Variability in earthquake stress drop and apparent stress, *Geophys. Res. Lett.*, *38*, L06303, doi:10.1029/2011GL046698.

Baltay, A. S., T. C. Hanks, and G. C. Beroza (2013), Stable stress-drop measurements and their variability: Implications for ground-motion prediction, *Bull. Seismol. Soc. Am.*, *103*, 211–222.

Boore, D. M., and G. M. Atkinson (1989), Spectral scaling of the 1985 to 1988 Nahanni, Northwest Territories, earthquakes, *Bull. Seismol. Soc. Am.*, *79*, 1736–1761.

Boore, D. M., J. P. Stewart, E. Seyhan, and G. M. Atkinson (2014), NGA-West2 equations for predicting PGA, PGV, and 5% damped PSA for shallow crustal earthquakes, *Earthquake Spectra*, *30*, 1057–1085.
Bryant, W. A., (compiler) (2005), Digital database of Quaternary and younger faults from the fault activity map of California, version 2.0. California Geological Survey. [Availale at http://www.consrv.ca.gov/CGS/information/ publications/QuaternaryFaults_ver2.]
Chiou, B. S. J., and R. R. Youngs (2008), An NGA model for the average horizontal component of peak ground motion and response spectra, *Earthquake Spectra*, *24*, 173–215.
Das, S., and C. H. Scholz (1981), Theory of time-dependent rupture in the Earth, *J. Geophys. Res.*, *86*, 6039–6051.
Dieterich, J. H. (1994), A constitutive law for the rate of earthquake production and its application to earthquake clustering, *J. Geophys. Res.*, *99*, 2601–2618.
Dieterich, J. H. (2007), Applications of rate- and state-dependent friction to models of fault slip and earthquake occurrence, in *Earthquake Seismology, Treatise on Geophysics*, vol. 4, edited by G. Shubert and H. Kanamori, pp. 107–129, Elsevier, Univ. of California.
Dieterich, J. H., and K. B. Richards-Dinger (2010), Earthquake recurrence in simulated fault systems, *Pure Appl. Geophys.*, *167*, 1087–1104.
Dieterich, J. H., and D. E. Smith (2009), Nonplanar faults: Mechanics of slip and off-fault damage, *Pure Appl. Geophys.*, *166*, 1799–1815.
Dunham, E. M., D. Belanger, L. Cong, and J. E. Kozdon (2011), Earthquake ruptures with strongly rate-weakening friction and off-fault plasticity. Part 2: Nonplanar faults, *Bull. Seismol. Soc. Am.*, *101*, 2308–2322.
Ely, G. P., S. M. Day, and J. B. Minster (2009), A support-operator method for 3-D rupture dynamics, *Geophys. J. Int.*, *177*, 1140–1150.
Felzer, K., R. Abercrombie, and G. Ekstrom (2004), A common origin for aftershocks, foreshocks, and multiplets, *Bull. Seismol. Soc. Am.*, *94*, 88–99.
Field, E. H., et al. (2014), Uniform California Earthquake Rupture Forecast, Version 3 (UCERF3)—The time-independent model, *Bull. Seismol. Soc. Am.*, *104*, 1122–1180.
Gerstenberger, M., S. Wiemer, and L. P. Jones (2005), Reasenberg, real-time forecasts of tomorrow's earthquakes in California, *Nature*, *435*, 328–331.
Gregor, N., et al. (2014), Comparison of NGA-West2 GMPEs, *Earthquake Spectra*, *30*, 1179–1197.
Helmstetter, A., and B. E. Shaw (2009), Afterslip and aftershocks in the rate-and-state friction law, *J. Geophys. Res.*, *114*, B01308, doi:10.1029/2007JB005077.
Helmstetter, A., and D. Sornette (2002), Diffusion of Epicenters of Earthquake Aftershocks, Omori's Law, and Generalized Continuous-Time Random Walk Models, *Phys. Rev. E*, *66*(6), 061104.
Helmstetter, A., Y. Kagan, and D. Jackson (2005), Importance of small earthquakes for stress transfers and earthquake triggering, *J. Geophys. Res.*, *110*, B05S08, doi:10.1029/2004JB003286.
Hickman, S. H., M. D. Zoback, and W. L. Ellsworth (2005), Structure and composition of the San Andreas fault zone at Parkfield: Initial results from SAFOD phases 1 and 2, *Eos Trans. AGU*, *87*(52), Fall Meet. Suppl., Abstract T2E–25.
Huc, M., and I. Main (2003), Anomalous stress diffusion in earthquake triggering: Correlation length, time dependence, and directionality, *J. Geophys. Res.*, *108*, 2324, doi:10.1029/2001JB001645.
Kagan, Y., and L. Knopoff (1981), Stochastic synthesis of earthquake catalogs, *J. Geophys. Res.*, *86*, 2853–2862.
Lin, G., P. M. Shearer, and E. Hauksson (2007), Applying a three-dimensional velocity model, waveform cross correlation, and cluster analysis to locate southern California seismicity from 1981 to 2005, *J. Geophys. Res.*, *112*, B12309, doi:10.1029/2007JB004986.
Madden, E. H., and D. D. Pollard (2012), Integration of surface slip and aftershocks to constrain the 3D structure of faults involved in the M 7.3 Landers earthquake, southern California, *Bull. Seismol. Soc. Am.*, *102*, 321–342.
Marsan, D., and O. Lengline (2008), Extending earthquakes' reach through cascading, *Science*, *319*, 1076–1079.
Ogata, Y. (1988), Statistical-models for earthquake occurrences and residual analysis for point-processes, *J. Am. Stat. Assoc.*, *83*, 9–27.
Perfettini, H., and J. P. Avouac (2007), Modeling afterslip and aftershocks following the 1992 Landers earthquake, *J. Geophys. Res.*, *112*, B07409, doi:10.1029/2006JB004399.
Power, W. L., T. E. Tullis, and J. D. Weeks (1988), Roughness and wear during brittle faulting, *J. Geophys. Res.*, *93*, 15268–15278, doi:10.1029/JB093iB12p15268.
Powers, P. M., and T. H. Jordan (2010), Distribution of seismicity across strike-slip faults in California, *J. Geophys. Res.*, *115*, B05305, doi:10.1029/2008JB006234.
Reasenberg, P., and L Jones (1989), Earthquake hazard after a mainshock in California, *Science*, *243*, 1173–1176.
Richards-Dinger, K., and J. H. Dieterich (2012), RSQSim earthquake simulator, *Seismol. Res. Lett.*, *83*, 983–990.
Schaff, D. P., G. H. R. Bokelmann, G. C. Beroza, F. Waldhauser, and W. L. Ellsworth (2002), High-resolution image of Calaveras fault seismicity, *J. Geophys. Res.*, *107*, 2186, doi:10.1029/2001JB000633.
Shaw, B. E. (1993), Generalized Omori law for aftershocks and foreshocks from a simple dynamics, *Geophys. Res. Lett.*, *20*, 907–910.
Shearer, P. (2002), Parallel Fault Strands at 9-km Depth Resolved on the Imperial Fault, Southern California, *Geophys. Res. Lett.*, *29*, 1674, doi:10.1029/2002GL015302.
Shearer, P. M. (2012a), Self-similar earthquake triggering, Bath's, law, and foreshock/aftershock magnitudes: Simulations, theory, and results for southern California, *J. Geophys. Res.*, *117*, B06310, doi:10.1029/2011JB008957.
Shearer, P. M. (2012b), Space-time clustering of seismicity in California and the distance dependence of earthquake triggering, *J. Geophys. Res.*, *117*, B10306, doi:10.1029/2012JB009471.
Smith, D. E., and J. H. Dieterich (2010), Aftershock sequences modeled with 3-D stress heterogeneity and rate-state seismicity equations: Implications for crustal stress estimation, *Pure Appl. Geophys.*, *167*, 1067–1085.
Sornette, D., and M. Werner (2005), Constraints on the size of the smallest triggering earthquake from the epidemic-type aftershock sequence model, Bath's law, and observed aftershock sequences, *J. Geophys. Res.*, *110*, B08304, doi:10.1029/2004JB003535.
Toda, S., R. Stein, K. Richards-Dinger, and S. Bozkurt (2005), Forecasting the evolution of seismicity in southern California: Animations built on earthquake stress transfer, *J. Geophys. Res.*, *110*, B05S16, doi:10.1029/2004JB003415.
van der Elst, N., and B. E. Shaw (2015), Larger aftershocks happen farther away: Nonseparability of magnitude and spatial distributions of aftershocks, *Geophys. Res. Lett.*, *42*, 5771–5778, doi:10.1002/2015GL064734.